

Modeling of a Type II Photofrin-mediated Photodynamic Therapy Process in a Heterogeneous Tissue Phantom

Xin-Hua Hu^{*1,2}, Yuanming Feng³, Jun Q. Lu¹, Ron R. Allison², Rosa E. Cuenca⁴, Gordon H. Downie⁵ and Claudio H. Sibata^{1,2}

¹Department of Physics, East Carolina University, Greenville, NC

²Department of Radiation Oncology, Brody School of Medicine, East Carolina University, Greenville, NC

³Department of Radiation Oncology, School of Medicine, University of Maryland, Baltimore, MD

⁴Department of Surgery, Brody School of Medicine, East Carolina University, Greenville, NC

⁵Department of Internal Medicine, Brody School of Medicine, East Carolina University, Greenville, NC

Received 4 May 2005; accepted 7 June 2005; published online 16 June 2005 DOI: 10.1562/2005-05-04-RA-513

ABSTRACT

We present a quantitative framework to model a Type II photodynamic therapy (PDT) process in the time domain in which a set of rate equations are solved to describe molecular reactions. Calculation of steady-state light distributions using a Monte Carlo method in a heterogeneous tissue phantom model demonstrates that the photon density differs significantly in a superficial tumor of only 3 mm thickness. The time dependences of the photosensitizer, oxygen and intracellular unoxidized receptor concentrations were obtained and monotonic decreases in the concentrations of the ground-state photosensitizer and receptor were observed. By defining respective decay times, we quantitatively studied the effects of photon density, drug dose and oxygen concentration on photobleaching and cytotoxicity of a photofrin-mediated PDT process. Comparison of the dependences of the receptor decay time on photon density and drug dose at different concentrations of oxygen clearly shows an oxygen threshold under which the receptor concentration remains constant or PDT exhibits no cytotoxicity. Furthermore, the dependence of the photosensitizer and receptor decay times on the drug dose and photon density suggests the possibility of PDT improvement by maximizing cytotoxicity in a tumor with optimized light and drug doses. We also discuss the utility of this model toward the understanding of clinical PDT treatment of chest wall recurrence of breast carcinoma.

INTRODUCTION

Photodynamic therapy (PDT) has attracted significant research efforts over the last two decades as an effective and viable modality for the treatment and management of superficial and luminal cancers by employing non-ionizing radiation of visible and near-

infrared light (1). Compared to radiation therapy and chemotherapy, the clinical benefits of PDT for patients include tumorcidal activity and potentially reduced side effects. Most photosensitizer (PS) drugs used in clinical studies of PDT achieve tumor eradication by generating highly reactive oxygen molecules in the singlet excited states through a Type II process. The three essential components in this process are photons, PS and oxygen molecules. The reactions among themselves and with cells and vascular systems are the key to understanding the cytotoxicity and tissue necrosis caused by PDT. Although numerous reports have been published on various aspects of PDT processes, including laboratory and clinical settings, quantitative modeling of the dynamic process remains a challenging problem to be solved. A modeling framework allowing for a clear understanding of the fundamental processes should help improve the clinical efficacy and expand the range of PDT.

Accurate modeling of PDT processes requires the establishment of a framework to consider cytotoxicity as the result of molecular interaction with the photons being distributed in tissues. It is difficult to determine light distribution in the illuminated zone because most human tissues are optically turbid and heterogeneous in their optical properties. The size of the zone is typically much larger than the wavelengths of the optical radiation in visible and near-infrared spectral regions, which renders extremely difficult the modeling of light as electromagnetic fields. A radiative transfer equation (2) provides an efficient tool for solving light distribution problems in turbid tissues at macroscopic scales using the optical parameters of an absorption coefficient μ_a , a scattering coefficient μ_s and a scattering phase function p . But it is impossible to find analytical solutions to radiative transfer problems with practical boundary conditions, and numerical methods are necessary. Heterogeneity in the optical properties of normal and tumor tissues within an illuminated zone demands multiple sets of optical parameters, further increasing the difficulty for optical modeling. The complex interaction of the molecules poses another challenge for PDT modeling in which many aspects are yet to be clearly understood and quantitatively characterized. For example, how does the relaxation of excited PS and oxygen molecules influence the cytotoxicity, and what is the effect of photon-PS interaction on the tissue optical properties? Despite these difficult questions, the clinical outcomes of PDT have demonstrated significant benefits in the treatment of certain types of cancers compared to conventional modalities (3). Clearly, a framework for modeling the complex PDT process will be

* To whom correspondence should be addressed: Department of Physics, East Carolina University, Greenville, NC 27858. Fax: 252-328-6314; e-mail: hux@mail.ecu.edu

Abbreviations: cw, continuous wave; HG, Henry-Greenstein; MC, Monte Carlo; PDT, photodynamic therapy; PS, photosensitizer.

© 2005 American Society for Photobiology 0031-8655/05

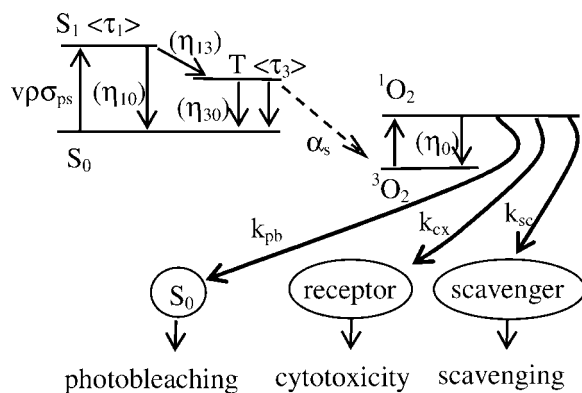


Figure 1. A schematic representation of the PDT process. The symbols in angled brackets are relaxation times of the excited states, symbols in parentheses are quantum efficiencies and symbols with dashed lines are reaction constants.

useful for comprehending the vast amount of data from *in vitro* research using cultured cells and *in vivo* studies in animal models and clinics.

Coupled rate equations have been employed to understand the change of oxygen concentrations in the triplet ground state (3O_2) and singlet excited state (1O_2) during PDT treatment of cultured cell spheroids (4,5) and cells (6). This approach was extended to model the variations of both PS concentration and light distribution in a homogeneous tissue phantom due to different exciting light beam parameters based on a diffusion approximation to the radiative transfer theory (7,8). A similar model was proposed to obtain the photobleaching dose constant by solving the decay of the PS concentration with one rate equation with the assumption of a simple exponential distribution of light fluence rate along the incident beam direction (9). In addition, PDT dosimetry under a pulsed illumination condition was studied with the diffusion model (10). These efforts were focused on the modeling of the photobleaching process, and therefore, quantitative relation between singlet oxygen production and cytotoxicity remains poorly understood. Accurate modeling of the PDT process to improve upon previous efforts represents a significant step toward optimization of the PDT planning process in which, for example, one can maximize tumor response and reduce side effects by fully using the difference between the cytotoxicity in tumor and normal tissues.

We present here our initial results in establishing a framework of PDT modeling by combining Monte Carlo (MC) simulations with solving rate equations to understand a Type II Photofrin-mediated PDT process. Light distributions in a heterogeneous tumor phantom were numerically obtained for different cases of tissue optical parameters to study the range of photon density. Literature on PDT research was surveyed to select values of coefficients and parameters for solving a set of coupled rate equations in the time domain to quantitatively analyze the dynamic process of PS activation by photons and subsequent cytotoxicity. The decay times of PS and unoxidized receptor concentrations were defined to investigate the dependence of photobleaching and cytotoxicity on drug dose and photon density. We also discuss the utility of the framework in illustrating previous clinical results of chest wall treatment by PDT.

MATERIALS AND METHODS

A Type II PDT process involves the excitation of PS by photons and a cascading chain of reactions with singlet oxygen as the intermediate,

leading to cytotoxicity and tissue necrosis. These events occur over drastically different spatial scales from the nanometer size of molecules to the millimeter size of photon scattering mean free path in the tissue. It has been demonstrated that diffusion can cause inhomogeneous distribution of oxygen at the micrometer scale of cells (4,5). Because we are primarily interested in the time dependence of the photodynamic process, the effect of oxygen diffusion and perfusion at the location \mathbf{r} is approximately accounted for with a rate of change P in the corresponding rate equation. For a continuous-wave (cw) light source, therefore, we can separately consider the spatial and temporal dependence of the PDT process: the spatial dependence of light distribution in tissues is obtained through MC simulations, whereas the time dependences of the concentrations of PS and oxygen molecules at \mathbf{r} are solved from a group of rate equations. The optical response of tissue and subsequent molecular interaction can be linked with the optical parameters of the tissue that are set as functions of both time and space. Because of the large difference between the spatial scales of molecular interaction and light distribution in tissue, the light distribution in terms of a photon density, $\rho(\mathbf{r})$, should be regarded as a local quantity averaged over the submillimeter size of multicell clusters.

We adopted a rate-equation approach first used by Foster *et al.* (4) to solve for the time dependence of the molecular concentrations in a Type II PDT process as a consequence of the local photon density $\rho(\mathbf{r})$ with six coupled, first-order differential equations. The PDT process is started by the absorption of photons by S_0 (the PS forms in their ground state) with an absorption cross-section, σ_{psa} . A schematic of the energy level diagram is presented in Fig. 1 to illustrate various pathways of the PDT process described by the rate equations. The concentrations of molecules in their ground and excited states are represented by their respective symbols in brackets and their rates of change are given by the following equations:

$$\frac{d[S_0]}{dt} = -v\rho\sigma_{psa}[S_0] - k_{pb}[^1O_2][S_0] + \frac{\eta_{10}}{\tau_1}[S_1] + \frac{\eta_{30}}{\tau_3}[T] + \frac{\alpha_s}{\tau_3}[T][^3O_2] \quad (1)$$

$$\frac{d[S_1]}{dt} = -\frac{1}{\tau_1}[S_1] + v\rho\sigma_{psa}[S_0] \quad (2)$$

$$\frac{d[T]}{dt} = -\frac{\eta_{30}}{\tau_3}[T] - \frac{\alpha_s}{\tau_3}[T][^3O_2] + \frac{\eta_{13}}{\tau_1}[S_1] \quad (3)$$

$$\frac{d[^3O_2]}{dt} = -\frac{\alpha_s}{\tau_3}[T][^3O_2] + \frac{\eta_o}{\tau_o}[^1O_2] + P \quad (4)$$

$$\frac{d[^1O_2]}{dt} = -k_{pb}[S_0][^1O_2] - k_{cx}[R][^1O_2] - k_{sc}[C][^1O_2] - \frac{\eta_o}{\tau_o}[^1O_2] + \frac{\alpha_s}{\tau_3}[T][^3O_2] \quad (5)$$

where 3O_2 and 1O_2 are oxygen in the ground and singlet-excited states ($^1\Delta_g$), S_1 and T are, respectively, PS in the singlet- and triplet-excited states and R is the intracellular receptor for 1O_2 . Use of the efficiency factor α_s instead of a k parameter for the bimolecular energy transfer from the excited PS to oxygen allows study of the effect of relaxation time τ_3 on the excitation of oxygen. Among these equations, (Eq. 5) describes the photochemical processes that produce and consume 1O_2 molecules. For example, the first and second terms on the right-hand side of (Eq. 5) are the rates of 1O_2 consumption in photobleaching and oxidization of intracellular receptors. In addition, (Eq. 5) also includes the reaction of 1O_2 with various oxygen scavengers with an average rate k_{sc} and concentration $[C]$. The values of coefficients and parameters are listed in Table I and a detailed discussion on selecting these values is presented in the next section.

It has been widely accepted that the cytotoxicity induced in a Type II PDT process is caused primarily by the oxidization of various intracellular receptors at the PS binding sites, including those of the vasculature in the tumor, with the highly active 1O_2 molecules (1,11). In response, various repair mechanisms can be activated within a cell to undo the cytotoxic damage. When the concentration of cytotoxic agents exceeds a certain threshold in a cell, irreversible apoptosis or necrosis occurs (12,13). Consequently, the time evolution of unoxidized receptors $[R]$ should be determined by its reaction rate with 1O_2 and a repair rate U as follows:

$$\frac{d[R]}{dt} = -k_{cx}[^1O_2][R] + U \quad (6)$$

As a result, the time dependence of $[R]$ can be related to cell survival in the time domain with a cell-killing model that is to be determined in the future.

Table 1. Values of the coefficients and parameters used in (Eq. 1) to (Eq. 6)

Symbol	Definition	Values	Notes and references
τ_1	Relaxation time of S_1 to S_0	10 ns	(28)
τ_3	Relaxation time of T to S_0	30 or 300 μ s	(29,30)
τ_0	Relaxation time of 1O_2 to 3O_2	30 or 300 ns	(29,30)
η_{10}	Quantum yield of S_1 transition to S_0	0.2	(32,33)
η_{13}	Quantum yield of S_1 transition to T	0.8	(32–34)
η_{30}	Quantum yield of T transition to S_0	0.3	(32–34)
η_0	Quantum yield of 1O_2 transition to 3O_2	0.3	(32,33)
α_s	Efficiency factor for energy transfer from T to 3O_2	1×10^{-17} (cm^3)	(4)
k_{pb}	Bimolecular photobleaching rate	2.0×10^{-10} ($\text{cm}^3 \cdot \text{s}^{-1}$)	It has been estimated in (4,5) that $k_{pb}/k_{cx}[R] \sim 80$ (M^{-1}), which yields a ratio k_{cx}/k_{pb} of about 15 if $[R] \sim [R]_i$ is assumed.
k_{cx}	Bimolecular cytotoxicity rate	2.0×10^{-9} ($\text{cm}^3 \cdot \text{s}^{-1}$)	Same as above.
k_{sc}	Bimolecular scavenging rate	1.0×10^{-9} ($\text{cm}^3 \cdot \text{s}^{-1}$)	See text.
V	Light speed in tissue = $v = c/n = c/1.38$	2.17×10^{10} ($\text{cm} \cdot \text{s}^{-1}$)	(48)
ρ	Photon density	From 5×10^4 to 5×10^7 (cm^{-3})	From MC simulations with incident irradiance of $I_0 = 200$ (mW/cm^2).
σ_{psa}	Absorption cross-section of S_0 molecules	5.0×10^{-13} (cm^2)	(26)
$[S_0]_i$	PS drug concentration in cells and tissues 48 h after injection	From 2×10^{10} to 2×10^{14} (cm^{-3})	See text.
$[S_1]_i$	Initial concentration of $[S_1]$	0	No excited PS at $t = 0$.
$[T]_i$	Initial concentration of $[T]$	0	No excited PS at $t = 0$.
$[^3O_2]_i$	Initial concentration of $[^3O_2]$	4.98×10^{17} or 5.06×10^{17} (cm^{-3})	(4,5)
$[^1O_2]_i$	Initial concentration of $[^1O_2]$	0	No excited oxygen at $t = 0$.
$[R]_i$	Initial concentration of intracellular molecular receptor available for binding with 1O_2	5.0×10^{17} (cm^{-3})	See text.
$[C]_i$	Scavenger concentration	1.0×10^3 (cm^{-3})	See text.
P	Rate of oxygen diffusion and perfusion	From 1.0×10^{12} to 1.0×10^{13} ($\text{cm}^{-3} \cdot \text{s}^{-1}$)	(5,35)
U	Cell damage repair rate	2.6×10^{12} ($\text{cm}^{-3} \cdot \text{s}^{-1}$)	Tested with a small value so that the repair effect can be neglected for $t < t_{\max}$

We point out that this model of the Type II PDT process presents a simplified picture of the actual PDT process consisting of different reacting molecules and receptors with a wide range of interactions. For example, the photobleaching or destruction of the PS can occur via two pathways depending on PS and its binding environment: one by photochemical reaction of S_0 with 1O_2 , and the other independent of oxygen (14). We limit our model on photobleaching to the former and described it by a reaction rate k_{pb} in (Eq. 5). It is also possible that multiple types of intracellular receptors exist that react with 1O_2 at different rates. Therefore, k_{cx} and $[R]$ should be regarded as the averaged values over different species of receptors involved in the PDT process. Despite these simplifications, different studies have demonstrated that the rate-equation approach provides a powerful tool for studying threshold problems of tissue damage by optical radiations such as PDT (4,5) and pulsed laser ablation (15). We thus believe that this approach will allow us to extract major characteristics of PDT without compromising the desired accuracy for explaining experimental data.

For cw light fields, a time-independent radiative transfer equation can be used to obtain light radiance $L(\mathbf{r}, \mathbf{s})$ at location \mathbf{r} in a direction \mathbf{s} within a tissue phantom as follows:

$$\frac{dL(\mathbf{r}, \mathbf{s})}{ds} = -\{\mu_a + \mu_s\}L(\mathbf{r}, \mathbf{s}) + \mu_s \int_{4\pi} p(\mathbf{s}, \mathbf{s}')L(\mathbf{r}, \mathbf{s}')d\Omega' \quad (7)$$

where $p(\mathbf{s}, \mathbf{s}')$ is the phase function describing the probability of light being scattered from \mathbf{s}' to \mathbf{s} (2). The light distribution in a turbid medium such as human tissues on a macroscopic scale can be accurately solved by a statistical method of MC simulations based on the equation above (16,17). We have developed and validated an MC code to track photons in tissue phantoms through stochastic processes characterized by $\mu_s(\mathbf{r})$, $\mu_a(\mathbf{r})$ and $p(\mathbf{s}, \mathbf{s}')$ (18–20). The basic algorithm uses a time-slicing method to efficiently tally the number of photons traversing through each cell of the computational grid dividing the tissue phantom after tracking each incident

photon (18). The output of our MC simulations are given in terms of a photon density function $\rho(\mathbf{r})$ within the tissue phantom that is related to light radiance $L(\mathbf{r}, \mathbf{s})$ in (Eq. 7) by the following equation:

$$\rho(\mathbf{r}) = \frac{\lambda \int_{4\pi} L(\mathbf{r}, \mathbf{s})d\Omega}{hv^2} \quad (8)$$

where h is the Planck constant, λ is the light wavelength and v is the light speed in the tissue. For PDT modeling, $\rho(\mathbf{r})$ should be interpreted as the local density of photons at the binding sites of PS. The function $\rho(\mathbf{r})$ can be a slow-varying function of time due to the changes in tissue optical parameters as discussed below. To find the range of photon density in an illuminated zone that includes both tumor and normal tissues, such as the case with chest wall treatment (3), we employed a heterogeneous tissue model with a rectangular-shaped tumor embedded in a semi-infinite phantom of the normal tissue. The tissue phantom is shown in Fig. 2 with a diverging laser beam delivered from an optical fiber overlapping with the z -axis. The Henyey-Greenstein (H-G) function, $p(\theta)$, was used as the phase function $p(\mathbf{s}, \mathbf{s}')$ in our MC code with the scattering angle θ between \mathbf{s} and \mathbf{s}' (21). The H-G function is fully characterized by an anisotropy factor g , which is equal to the mean value of $\cos\theta$. The heterogeneous tumor tissue phantom is described by μ_s and μ_a in the tumor region and by μ_{s0} and μ_{a0} in the normal tissue region. We assumed the same values of anisotropy factor g and refractive index n for both tumor and normal tissue regions.

The differences in the optical parameters between tumor and normal tissues can be attributed to the physiological variations such as the extravasculature in the tumor and different PS uptake. Literature on the correlation between PS concentration and values of optical parameters of different tissues is quite limited. *In vivo* measurements of light radiance distribution in human subjects and animal models injected with different forms of PS can be inverted to obtain optical parameters based on

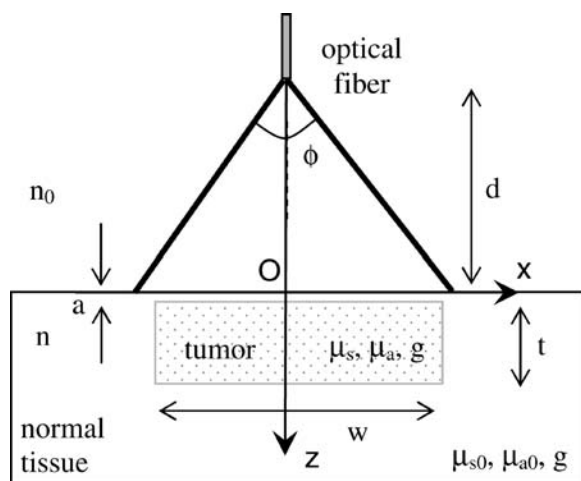


Figure 2. The configuration of the heterogeneous tissue phantom with a rectangular tumor embedded in a semi-infinite phantom of normal tissue. A uniform profile was assumed for the incident beam with $\phi = 60^\circ$, $d = 34.6$ mm and beam diameter at the phantom surface was given as 40.0 mm. The optical parameters for the normal tissue region were assumed to be (μ_{a0}, μ_{s0}) , whereas for the tumor region (μ_a, μ_s) with the same anisotropy factor $g = 0.80$ and refractive index $n = 1.38$. Other parameters are $w = 28.0$ mm, $t = 3$ mm, $a = 0.5$ mm and $n_0 = 1.00$ for the refractive index of air.

a diffusion approximation of the radiative equation (22–24). These results suggested that μ_a is linearly related to the drug dose of PS in the tissues, whereas the reduced scattering coefficient $\mu_s' = \mu_s(1-g)$ appears to be independent of the PS concentration at or near the wavelength corresponding to the absorption peak of PS. It has been found, however, that both optical parameters μ_a and μ_s' can be different in normal and tumor tissues due to different hemoglobin concentration and saturation (23,25). On the basis of these results, we considered two cases of different values of μ_a and μ_s in the normal and tumor regions of the tissue phantom to model tissue heterogeneity. Among these differences, we assumed that μ_a relates to the PS uptake as follows:

$$\mu_a = \mu_{a0} + \sigma_{psa}[S_0] \quad (9)$$

Equation 9 can also be used to check the consistency between the values of μ_a and μ_{a0} used in the MC simulations and σ_{psa} in the rate equations for a given value of $[S_0]$.

RESULTS

We chose a PS of porphyrin type such as Photofrin[®] for our model calculations for its status as the most established clinical PS. When data were not available, results reported with other PS types were used as the basis for selecting the appropriate values of the coefficients in (Eq. 1) to (Eq. 7), as discussed below and noted in Table 1. It is well known that the molecular parameters of PDT processes vary in different cells and their environments and, therefore, uncertainty exists for choosing the parameter values. Consequently, one objective of this study was to test the ranges of critical parameter values so that the output from our model can be related to the results of cell and clinical studies.

We first investigated the range of photon density variation in the heterogeneous tissue phantom shown in Fig. 2 with our MC code based on (Eq. 7) and (Eq. 8) using the anisotropy factor $g = 0.80$ and refractive index $n = 1.38$ for both tumor and normal tissue regions. Other parameters of the phantom and the incident beam are given in the caption for Fig. 2. The ranges of the tissue optical parameters were selected based on the values determined from bloodless porcine skin dermis tissues (26) plus blood (27) at light wavelength

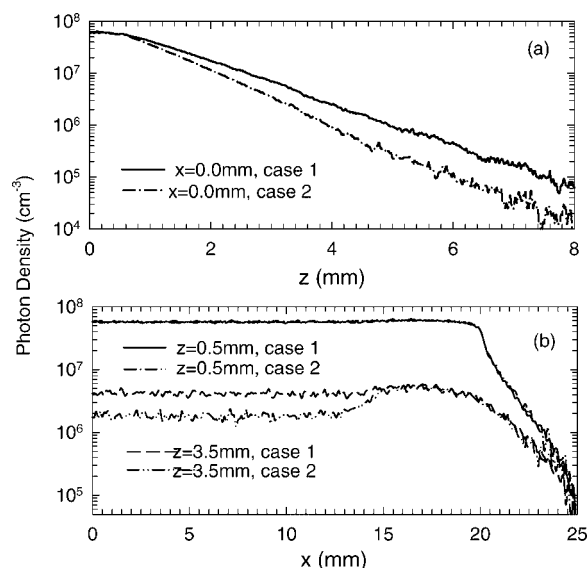


Figure 3. Photon density along the (a) z-axis and (b) x-axis in the tissue phantom depicted in Fig. 2. The optical parameters for the normal tissue are: $\mu_{a0} = 0.20$ mm⁻¹, $\mu_{s0} = 5.0$ mm⁻¹. Two cases of tumor were considered: case 1, $\mu_a = 0.24$ mm⁻¹, $\mu_s = 6.0$ mm⁻¹; and case 2: $\mu_a = 0.40$ mm⁻¹, $\mu_s = 10.0$ mm⁻¹. In both cases, the same values of $g = 0.80$ and $n = 1.38$ were assumed for normal and tumor tissue regions.

$\lambda \sim 630$ nm. A total of 2.12×10^8 photons in a diverging beam of light have been tracked within the tissue phantom to obtain the spatial distribution of photon density $\rho(\mathbf{r})$ on one node of our parallel computing cluster with a xeon 3.06 GHz CPU. Each MC simulation took between 30 and 40 min to complete, depending on the tissue parameters. Assuming an incident irradiance delivered to the air side of tissue surface as $I_0 = 200$ mW/cm², the MC-simulated photon densities are shown in Fig. 3 along the z- and x-axes, which are scaled according to I_0 . In the normal tissue region, we adopted the values of $\mu_{a0} = 0.20$ mm⁻¹ and $\mu_{s0} = 5.0$ mm⁻¹ based primarily on our recent results of *in vitro* measurements of the porcine skin dermis (26) and hemoglobin absorption data (27). Due to the limited size and large fluctuation of *in vivo* data on tissue optical parameters, two cases of tumor were considered for studying the effects of different μ_s -induced and PS-induced changes in μ_a on light distribution: $\sigma_{psa}[S_0] = 0.2\mu_{a0} = 0.04$ mm⁻¹, $\mu_s = 6.0$ mm⁻¹ and $\sigma_{psa}[S_0] = \mu_{a0} = 0.20$ mm⁻¹, $\mu_s = 10.0$ mm⁻¹. In both cases, we assumed that $[S_0]$ in the tumor region correspond to an injected dose of 2 mg/kg. The large fluctuation in small values for ρ is due to the variance in the MC results tracking a finite number of photons. For the region on top of the tumor ($z \leq 0.5$ mm) the photon distributions ρ in the two cases were nearly identical, as expected. But $\rho(0, 0, z)$ within the tumor between $z = 0.5$ and 3.5 mm varies between 5.7×10^7 cm⁻³ and 1.8×10^6 cm⁻³ along the z-axis for the second case of $\sigma_{psa}[S_0] = \mu_{a0}$. The photon density variation in the x-y plane is much smaller within the tumor than that along the z-axis because of the uniform beam profile assumed for the diverging incident beam. These results demonstrate that variation in ρ is significant in the treated zone of a typical superficial tumor, by a factor of up to 30.

The system of the rate equations from (Eq. 1) to (Eq. 6) was solved to obtain the time dependence of various concentrations corresponding to the different locations inside the tissue phantom. We used an ordinary differential equation solver within the Matlab platform (ode15s of Matlab 6.5, MathWorks, Inc.) for a stiff system of equations with different time steps between 0 ns and t_{max}

= 3000 s to achieve desired accuracy within the memory limit of the computer. Values of various coefficients and parameters were selected for the numerical solutions based on published reports, which are summarized below and listed fully in Table 1.

The relaxation time of PS from S_1 to S_0 is given by τ_1 , which has been estimated and measured (28) to be about 10 ns due to the fast transitions between the singlet states. In contrast, the relaxation time of the PS for intersystem crossing from T to S_0 , τ_3 , has been reported to be ranging from microseconds to milliseconds (29–31) and two values of 30 or 300 μ s for τ_3 were examined in our modeling study. Fast relaxation of the singlet oxygen has been noted widely with τ_0 estimated to be about less than 1 μ s (29,30). We adopted $\tau_0 = 30$ ns in our calculations. The quantum yields of the S_1 to S_0 , T to S_0 for the PS and the 1O_2 to 3O_2 were set as $\eta_{10} = 0.2$, $\eta_{30} = 0.3$ and $\eta_0 = 0.3$, respectively (32–34), which led to $\eta_{13} = 1 - \eta_{10} = 0.8$. For simplicity, constant values were used for the rate of oxygen diffusion and perfusion P in (Eq. 4), the scavenger concentration, $[C] = [C]_i$, in (Eq. 5) and the repair rate U in (Eq. 6). The value of P in (Eq. 4) was estimated from the reported values of oxygen diffusion constant (35) and oxygen concentration derivatives (5) based on cultured cell or spheroid measurements. Because no experimental data could be found, we used a small value of $k_{sc}[C]_i$ for this report, which had minimal influence on $[^1O_2]$ and $[R]$ over the time window of t_{max} . Study of the detailed forms of P and $k_{sc}[C]_i$ as functions of time, their effects on solutions of rate equations and comparison with PDT treatment of cultured cells is currently in progress.

The initial value of the PS drug concentration $[S_0]_i$ in tumors was derived by relating linearly to the typical injected dose of 2 mg/kg for Photofrin[®] with a molecular weight of about 3000 (d) (36). This yields a maximum body-average concentration of about 4×10^{14} cm^{-3} . Considering that the actual concentration of PS in cells and tissues can vary in a large range at the time of light treatment, 48 h after injection, the values of $[S_0]_i$ was therefore set to change between 2×10^{10} and 2×10^{14} cm^{-3} in our calculations. Only results for a portion of the above range, between 2×10^{11} and 2×10^{12} cm^{-3} , are presented in Figs. 5 and 6 in which significant variation of delay times could be observed. Hydrophobic PS drugs, including Photofrin[®], can localize in mitochondrial membranes as the primary binding sites for PDT-induced apoptosis with high affinity for peripheral benzodiazepine receptors (37–39). Therefore, the initial value of $[R]$ for the intracellular concentration of singlet oxygen receptors was estimated from the morphological structure of the mitochondria. On the basis of an ultrastructural analysis of normal rat Leydig cells, it has been determined that the total area of mitochondrial membrane per cell is approximately around 3000 μm^2 (40). By choosing the thickness of the membrane to be about 10 nm and the receptors' molecular weight at about 3000 (d), we set $[R]_i$ to be 5×10^{17} cm^{-3} . The values of other parameters and initial values of concentrations were estimated through a similar process and are noted in Table 1. These initial estimations of the parameters will be improved continuously in the future as more relevant experimental results are identified in literature and acquired through our own laboratory studies.

The time dependences of PS, oxygen and receptor concentrations have been calculated for two different values of τ_3 and are shown in Fig. 4 with $t = 0$ as the starting time of the incident light. These concentrations demonstrate two types of behaviors: those for the ground-state molecules of PS, oxygen and unoxidized receptors are slow-varying in response to the activation light, whereas those for the excited molecules exhibit transient responses depending

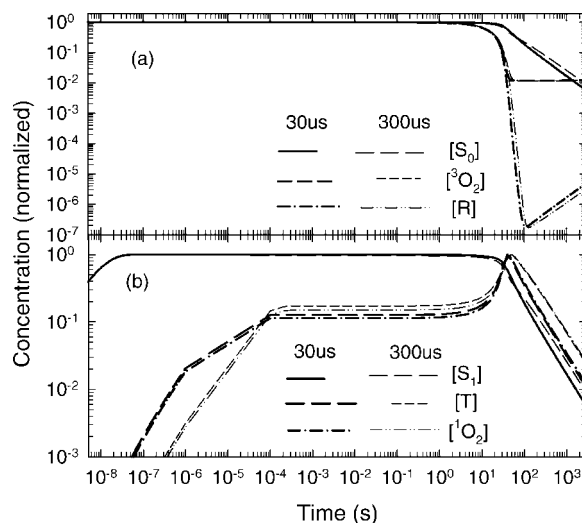


Figure 4. The time dependence of the concentrations of (a) PS and oxygen molecules in ground state and unoxidized receptor; (b) excited molecules for $\tau_3 = 30$ and 300 μ s. The parameters were set as $[^3O_2]_i = 5.06 \times 10^{17}$ (cm^{-3}), $[S_0]_i = 5.00 \times 10^{13}$ (cm^{-3}), $\rho = 1.00 \times 10^5$ (cm^{-3}). For $[S_0]$, $[^3O_2]$ and $[R]$ the concentrations are normalized by their initial values while for $[S_1]$, $[T]$ and $[^1O_2]$ the concentrations are normalized by their maximum values of $[S_1]_m = 2.59 \times 10^9$ (cm^{-3}), $[T]_m = 9.84 \times 10^{11}$ (cm^{-3}) and $[^1O_2]_m = 1.84 \times 10^7$ (cm^{-3}), respectively.

on the specific choice of relaxation times. The time dependences of normalized $[S_0]$ can be related to the experimental data of fluorescence *in vivo* or transient absorbance *in vitro*, while that of $[R]$ in comparison with the illumination time t_{max} can be related to the survival probability of cultured cells under PDT treatment through an appropriate cell-killing model. Therefore, we analyzed the time dependence of the two concentrations as the indicators of photobleaching and cytotoxicity in our PDT model. With these analyses, we defined the decay times of $[S_0]$ and $[R]$ below as the quantitative parameters for characterization of the photobleaching and cytotoxicity.

The concentration of the unoxidized receptors $[R]$ shown in Fig. 4 remains at its initial value followed by a steep decrease that can be described by a power law as t^{-p} , with p ranging from 10 to 12. When $[R]$ is reduced to about 10^{-5} of its initial value, the repair term U in (Eq. 6) starts to dominate for $t > 30$ s. The PS concentration $[S_0]$ follows a similar monotonically decreasing trend in the time domain with a less steep slope. Therefore, we define two decay times, t_s and t_R , as the times for $[S_0]$ and $[R]$ to be reduced to 1% of their initial values;

$$[S_0](t_s) = 0.01[S_0](0) \quad (10)$$

$$[R](t_R) = 0.01[R](0) \quad (11)$$

where $[S_0](0)$ and $[R](0)$ are the initial values of $[S_0]$ and $[R]$, respectively, at $t = 0$. These decay times are functions of initial drug dose and irradiance of incident light in terms of $[S_0]_i$ and ρ at the binding locations and thus were used to quantitatively study the phenomena of photobleaching and cytotoxicity in our modeling study. For example, it is easy to see in Fig. 4 that the value of τ_3 primarily affects the transient behavior of the excited molecules. We also investigated the effect of different O_2 relaxation time with $\tau_0 = 30$ or 300 ns (not shown) and found that their effect on t_s and t_R is negligible. For the following results the values of $\tau_3 = 300$ μ s and $\tau_0 = 30$ ns were adopted. Similar calculations were carried out to select the appropriate values of the parameters P and U.

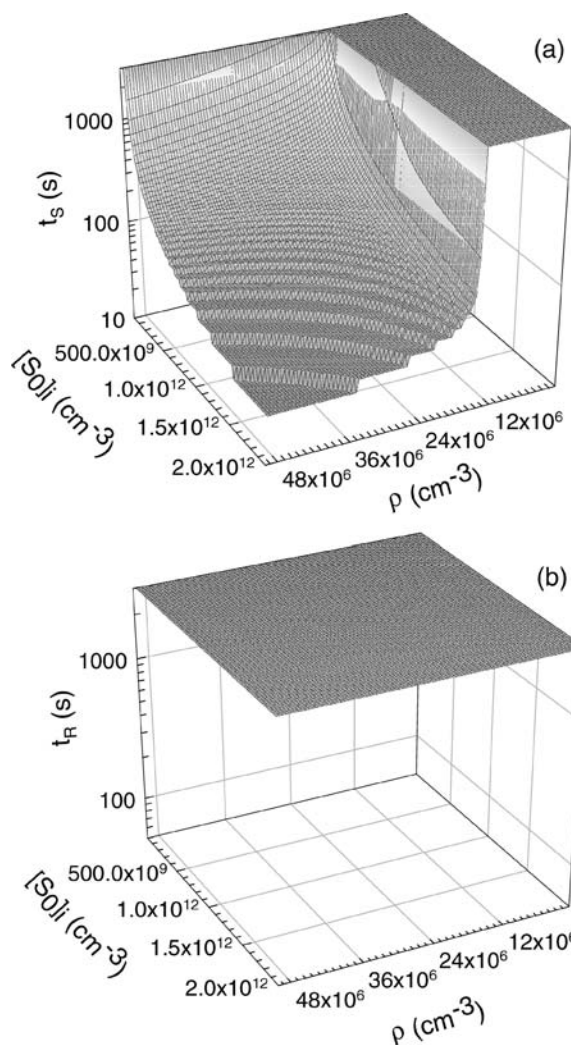


Figure 5. The 3-D plot of the decay times, defined in (Eq. 10) and (Eq. 11), as a function of $[S_0]_i$ and ρ : (a) t_s for $[S_0]_i$; (b) t_R for $[R]$. The initial concentration of the ground-state oxygen was set as $[^3O_2]_i = 4.98 \times 10^{17}$ (cm⁻³), and other parameters are listed in Table 1.

By solving (Eq. 1) to (Eq. 6) in the time domain for different values of $[S_0]_i$ and ρ , we obtained the decay times t_s and t_R as the functions of these two variables to numerically study the processes of photobleaching and cytotoxicity. The effect of different initial oxygen concentrations was first investigated and a threshold of initial value of oxygen $[^3O_2]_i$ was identified under which the cytotoxicity is blocked ($t_R > t_{max}$) while photobleaching still occurs. Two cases are shown in Figs. 5 and 6 in which the decay times are plotted as the functions of $[S_0]_i$ and ρ with different $[^3O_2]_i$. When $[^3O_2]_i < 5 \times 10^{17}$ cm⁻³, $[R]$ always remains above 1% of its initial value for $t < t_{max}$. Once $[^3O_2]_i$ exceeds the threshold value, t_R decreases to about 70 s for maximal $[S_0]_i$ and ρ , as shown in Fig. 6, and these results are not sensitive to $[^3O_2]_i$. In contrast, the decay time t_s is quite similar in both cases, decreasing from above 3000 s for small $[S_0]_i$ and ρ to about 30 s for large $[S_0]_i$ and ρ .

DISCUSSION

With more than two decades of active research, significant progress has been made to understand the fundamental photochemical and

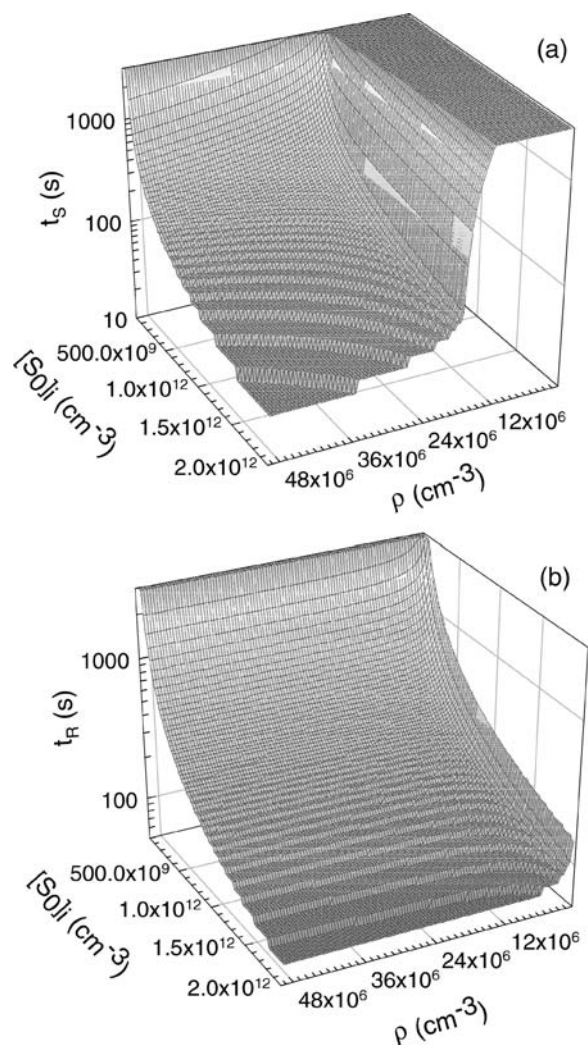


Figure 6. Same as Fig. 5 with $[^3O_2]_i = 5.06 \times 10^{17}$ (cm⁻³).

photobiological mechanisms underlying PDT. Despite the potential benefits that have been well recognized (1), PDT remains an underutilized treatment modality for patients with cancer. Major problems, in our view, may be related to the lack of tools to quantitative model light dosimetry and monitor PDT processes in clinics for optimized and reproducible response by patients. To overcome these difficulties, accurate models of PDT and tissue optics need to be developed. This report represents our first step toward this long-term goal by providing a framework to numerically study the light dosimetry in heterogeneous tissue phantom and its effect on cytotoxicity and photobleaching in a PDT process. Future improvement of modeling accuracy and efficiency with increased accuracy in rate equation parameters and parallel computing should help the expansion of PDT in the treatment and management of patients with cancer.

Current assessments of light dosimetry in PDT clinics are limited to the measurement of irradiance I_0 of the incident light beam and calculation of related fluence, $F = \int_0^{t_{max}} I_0(t) dt = I_0 t_{max}$ for an exposure time t_{max} where I_0 is assumed as a constant for a cw light source. The MC method allows accurate calculations of the local photon density $\rho(\mathbf{r})$ from a given I_0 , beam profile and tissue optical parameters. As we have shown in the coupled rate equations from (Eq. 1) to (Eq. 6), it is the $\rho(\mathbf{r})$ that directly determines a local PDT

process in a tissue. For $t < t_S$, $\rho(\mathbf{r})$ can be regarded as a steady-state distribution because the tissue optical parameters remain essentially the same because of negligible photobleaching. The results shown in Fig. 3 demonstrate a large variation in photon density in the embedded tumor within the first few millimeters of the surface. This requires the consideration of the PDT process as a local event. We point out that the density of absorbed photons $\rho_a(\mathbf{r})$ should not be confused with $\rho(\mathbf{r})$, which consists of the photons present at \mathbf{r} . The two densities are related by the following equation:

$$\rho_a(\mathbf{r}) = \int_0^{t_{\max}} \nu \rho(\mathbf{r}) \mu_a(\mathbf{r}, t) dt \quad (12)$$

where μ_a is due to the absorption of photons by PS and other chromophores.

The problem of quantitative modeling of cell-killing by singlet oxygen in a Type II PDT process remains unsolved. From the time evolution of unoxidized receptor concentration within a cell we extract a decay time t_R in an attempt to characterize the cytotoxicity with a single parameter. Although cytotoxicity could be triggered well before the 1% of $[R]_i$ ($=[R](0)$) is reached, the steep decrease in $[R]$ for $t \sim t_R$ (see Fig. 4) indicates that t_R is insensitive to the choice of exact percentage. As a result, t_R was used as a marker for the start of the cell-killing process to investigate the cytotoxicity of PDT as a function of $\rho(\mathbf{r})$ and $[S_0]_i$. A somewhat different time evolution can be observed for $[S_0]_i$, but a decay time t_S can still be used as an indicator of PS drug depletion due to photobleaching. Comparing the decay times with the illumination time t_{\max} allows a quantitative test of our model against experimental data of PDT studies in controlled environments such as cultured cells. For example, the dependence of the ratio t_R/t_{\max} on fluence, PS drug concentration and oxygen concentration can be related to the cell survival ratio and other parameters.

The results of our PDT model calculations exhibit a sensitivity to $[^3O_2]_i$ at the value of about $5.0 \times 10^{17} \text{ cm}^{-3}$, which corresponds to a concentration of 0.8 mM in the cytoplasm. For $[^3O_2]_i < 5.0 \times 10^{17} \text{ cm}^{-3}$ we found that the cytotoxicity is effectively blocked for the studied ranges of $[S_0]_i$ and ρ , as shown in Fig. 5. Once $[^3O_2]_i$ was set to a value above $5.0 \times 10^{17} \text{ cm}^{-3}$, however, t_R rapidly decreases as $[S_0]_i$ and ρ increases, as shown in Fig. 6, and the data for t_R become insensitive to the actual value of $[^3O_2]_i$. These results are consistent with the well-known effect of oxygen and condition of hypoxia on cytotoxicity (41,42) and the insensitivity of tumor cell survival ratios to the conditions of normobaric carbogen, and normobaric and hyperbaric oxygenation (43) in PDT. It is interesting to note from Fig. 6 that $t_S < t_R$ for most combinations of $[S_0]_i$ and ρ . This indicates that combinations of PS drug and light doses may be explored to achieve cytotoxicity in a tumor without significant photobleaching. The effect of oxygen diffusion and perfusion was negligible in these calculations because of small P (see Table 1), which led to total contribution to $[^3O_2]_i$ by diffusion and perfusion to be less than 1% of $[^3O_2]_i$ over a time window of 3000 s. We also studied the cases with P increased by factors of 5, 10 and 20 and found the results presented in Fig. 5 and 6 remain about the same.

PDT has been studied as a salvage procedure for patients with chest wall recurrence of breast carcinoma who failed multiple treatments by other modalities (3,44). Significant improvement in tumor response and reduction in post-treatment cutaneous morbidity rate was achieved with a low Photofrin dose of 0.8 mg/kg (3) and a mean total incident fluence of 150 J/cm² in comparison with a standard dose of 2 mg/kg (45,46). The incident

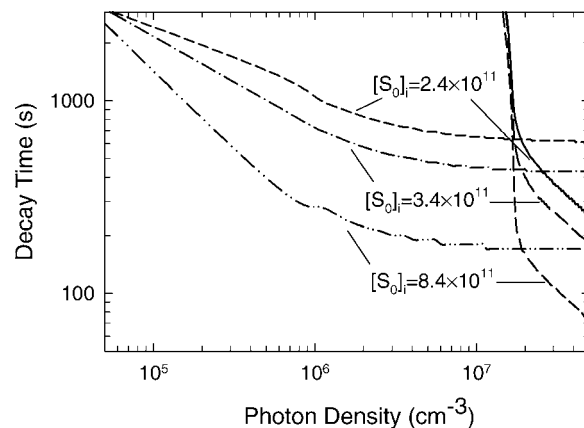


Figure 7. The decay time of t_S (solid and dash lines) and t_R (short dash and dash-dot lines) versus the photon density at different values of $[S_0]_i$.

fluences used were up to 300 J/cm² at irradiances up to 150 mW/cm². The choice of 0.8 mg/kg for the Photofrin dose was based on the observed clinical dose threshold of 0.57 mg/kg for minimal tumor response. The improved tumor response to PDT treatment with low Photofrin dose has been attributed to the adoption of relatively large illumination margin around the visible/palpable lesions and much-reduced necrosis in the surrounding normal tissues (3). These clinical results can be explained by our PDT model calculations displayed in Fig. 7 for the case of sufficient oxygen supply that can be assumed for the treatment of superficial lesions of chest wall. Because the total incident fluence of 150 J/cm² was obtained with $I_0 = 150 \text{ mW/cm}^2$ for an illumination time $t_{\max} = 1000 \text{ s}$, the corresponding photon density ρ would vary from 1.4×10^6 to $4.3 \times 10^7 \text{ cm}^{-3}$ within the tumor on the z-axis in the phantom shown in Fig. 2. If we assume that the observed threshold of Photofrin dose at 0.57 mg/kg correspond to $[S_0]_i = 2.4 \times 10^{11} \text{ cm}^{-3}$ in our model where the decay time t_R is approximately the same with t_{\max} , then the doses of 0.8 and 2.0 mg/kg correspond to $[S_0]_i = 3.4 \times 10^{11} \text{ cm}^{-3}$ and $[S_0]_i = 8.4 \times 10^{11} \text{ cm}^{-3}$ for a linear relation between $[S_0]_i$ and injected drug dose. The decay times of t_R and t_S are plotted as functions of ρ in Fig. 7 for three cases. In comparison with the drug dose of 0.8 mg/kg, the use of 2.0 mg/kg substantially increases the range of ρ in which $t_R < t_{\max}$ is satisfied and thus may lead to severe necrosis of normal tissues in the margin of tumor. This indicates that the practice of using low drug dose slightly above the threshold of tumor response could improve the prognosis of the patients by reducing the collateral tissue damage without compromising the killing of tumor cells.

For the results presented in this report, we assumed that $[S_0]$ does not change notably over the time window of interest due to photobleaching effect so that μ_a in (Eq. 9) can be treated as constants. This is certainly the case for $t \ll t_S$ or the negligible contribution to μ_a by $[S_0]$. For other cases in our discussions it has been verified that the changes of ρ due to different $[S_0]$ were very small in comparison to its value at $t = 0$ on the z-axis of the tissue phantom. We also note that our model is capable of taking into account the time dependence of $[S_0]$ by updating $[S_0]$ in (Eq. 9) to obtain current values of optical parameters in the MC simulations and ρ in (Eq. 1) alternatively in the time domain. Because $[S_0]$ varies slowly in the time domain, this procedure of real-time solution of our model can be accomplished with multiple MC simulations in which each can be completed within 40 min on a single computer of 3.04 GHz CPU for tracking 2.12×10^8 photons.

Preliminary results of parallel MC simulations (47) indicated that the simulation time can be reduced to less than 3 min on a computing cluster of 16 processing elements with the same CPUs.

In summary, we have demonstrated the feasibility of modeling a Type II Photofrin-mediated PDT process by solving a set of rate equations to obtain the time dependence of the PS, oxygen and intracellular unoxidized receptors. Light distributions in a heterogeneous tissue phantom were calculated using an MC method. Based on these results, decay times were defined for the concentrations of the PS drug and receptors as the metrics to characterize photobleaching and cytotoxicity. With this approach we calculated the decay times as the functions of the drug dose and photon density at different concentrations of oxygen, which can be used to quantitatively investigate the photobleaching and cytotoxicity effect. A threshold of oxygen was identified in our model under which no cytotoxicity can be observed and the decay times become insensitive to the oxygen concentration once it exceeds the threshold. The potential clinical utility of this PDT model is exemplified in the explanation of patient outcomes from PDT treatment of chest wall recurrence of breast carcinoma.

REFERENCES

- Dougherty, T. J., C. J. Gomer, B. W. Henderson, G. Jori, D. Kessel, M. Korbelik, J. Moan and Q. Peng (1998) Photodynamic therapy. *J. Natl. Cancer Inst.* **90**, 889–905.
- Chandrasekhar, S. (1960) *Radiative transfer*. Dover Publications, New York.
- Allison, R., T. Mang, G. Hewson, W. Snider and D. Dougherty (2001) Photodynamic therapy for chest wall progression from breast carcinoma is an underutilized treatment modality. *Cancer* **91**, 1–8.
- Foster, T. H., R. S. Murrant, R. G. Bryant, R. S. Knox, S. L. Gibson and R. Hilf (1991) Oxygen consumption and diffusion effects in photodynamic therapy. *Radiat. Res.* **126**, 296–303.
- Georgakoudi, I., M. G. Nichols and T. H. Foster (1997) The mechanism of Photofrin photobleaching and its consequences for photodynamic dosimetry. *Photochem. Photobiol.* **65**, 135–144.
- Dysart, J. S., G. Singh and M. S. Patterson (2005) Calculation of singlet oxygen dose from photosensitizer fluorescence and photobleaching during mTHPC photodynamic therapy of MLL cells. *Photochem. Photobiol.* **81**, 196–205.
- Pogue, B. W., R. W. Redmond and T. Hasan (1996) Dosimetry for pulsed laser photodynamic therapy. *Proc. SPIE* **2681**, 130–139.
- Farrell, T. J., R. P. Hawkes, M. S. Patterson and B. C. Wilson (1998) Modeling of photosensitizer fluorescence emission and photobleaching for photodynamic therapy dosimetry. *Appl. Opt.* **37**, 7168–7183.
- Jongen, A. J. and H. J. Sterenborg (1997) Mathematical description of photobleaching in vivo describing the influence of tissue optics on measured fluorescence signals. *Phys. Med. Biol.* **42**, 1701–1716.
- Pogue, B. W., L. Lilje, M. S. Patterson, B. C. Wilson and T. Hasan (1997) Absorbed photodynamic dose from pulsed versus continuous wave light examined with tissue-simulating dosimeters. *Appl. Opt.* **36**, 7257–7269.
- Peng, Q., J. Moan and J. M. Nesland (1996) Correlation of subcellular and intratumoral photosensitizer localization with ultrastructural features after photodynamic therapy. *Ultrastruct. Pathol.* **20**, 109–129.
- Agarwal, M. L., M. E. Clay, E. J. Harvey, H. H. Evans, A. R. Antunez and N. L. Oleinick (1991) Photodynamic therapy induces rapid cell death by apoptosis in L5178Y mouse lymphoma cells. *Cancer Res.* **51**, 5993–5996.
- Luo, Y. and D. Kessel (1997) Initiation of apoptosis versus necrosis by photodynamic therapy with chloroaluminum phthalocyanine. *Photochem. Photobiol.* **66**, 479–483.
- Georgakoudi, I. and T. H. Foster (1998) Singlet oxygen- versus nonsinglet oxygen-mediated mechanisms of sensitizer photobleaching and their effects on photodynamic dosimetry. *Photochem. Photobiol.* **67**, 612–625.
- Fang, Q. and X. H. Hu (2004) Modeling of skin tissue ablation by nanosecond pulses from ultraviolet to near-infrared and comparison with experimental results. *IEEE J. Quant. Electro.* **40**, 69–77.
- Wilson, B. C. and G. Adam (1983) A Monte Carlo model for the absorption and flux distributions of light in tissue. *Med. Phys.* **10**, 824–830.
- Wang, L., S. L. Jacques and L. Zheng (1997) CONV—convolution for responses to a finite diameter photon beam incident on multi-layered tissues. *Comput. Methods Programs Biomed.* **54**, 141–150.
- Song, Z., K. Dong, X. H. Hu and J. Q. Lu (1999) Monte Carlo simulation of converging laser beams propagating in biological materials. *Appl. Opt.* **38**, 2944–2949.
- Du, Y., X. H. Hu, M. Cariveau, X. Ma, G. W. Kalmus and J. Q. Lu (2001) Optical properties of porcine skin dermis between 900 nm and 1500 nm. *Phys. Med. Biol.* **46**, 167–181.
- Ma, X., J. Q. Lu, R. S. Brock, K. M. Jacobs, P. Yang and X. H. Hu (2003) Determination of complex refractive index of polystyrene microspheres from 370 to 1610 nm. *Physics Med. Biol.* **48**, 4165–4172.
- Henyey, L. G. and J. L. Greenstein (1941) Diffuse radiation in the galaxy. *Astrophys. J.* **93**, 70–83.
- Chen, Q., B. C. Wilson, S. D. Shetty, M. S. Patterson, J. C. Cerny and F. W. Hetzel (1997) Changes in *in vivo* optical properties and light distributions in normal canine prostate during photodynamic therapy. *Radiat. Res.* **147**, 86–91.
- Pham, T. H., R. Hornung, M. W. Berns, Y. Tadir and B. J. Tromberg (2001) Monitoring tumor response during photodynamic therapy using near-infrared photon-migration spectroscopy. *Photochem. Photobiol.* **73**, 669–677.
- Zhu, T. C., A. Dimofte, J. C. Finlay, D. Stripp, T. Busch, J. Miles, R. Whittington, S. B. Malkowicz, Z. Tochner, E. Glatstein and S. M. Hahn (2005) Optical properties of human prostate at 732 nm measured in mediated photodynamic therapy. *Photochem. Photobiol.* **81**, 96–105.
- Fantini, S., S. A. Walker, M. A. Franceschini, M. Kaschke, P. M. Schlag and K. T. Moesta (1998) Assessment of the size, position, and optical properties of breast tumors in vivo by noninvasive optical methods. *Appl. Opt.* **37**, 1982–1989.
- Ma, X., J. Q. Lu, H. Ding and X. H. Hu (2005) Bulk optical parameters of porcine skin dermis tissues at 8 wavelengths from 325 to 1557 nm. *Opt. Lett.* **30**, 412–414.
- Van Assendelft, O. W. (1970) *Spectrophotometry of Haemoglobin Derivatives*. C.C. Thomas, Springfield, IL.
- Kress, M., T. Meier, R. Steiner, F. Dolp, R. Erdmann, U. Ortmann and A. Ruck (2003) Time-resolved microspectrofluorometry and fluorescence lifetime imaging of photosensitizers using picosecond pulsed diode lasers in laser scanning microscopes. *J. Biomed. Opt.* **8**, 26–32.
- Moan, J. and K. Berg (1991) The photodegradation of porphyrins in cells can be used to estimate the lifetime of singlet oxygen. *Photochem. Photobiol.* **53**, 549–553.
- Niedre, M., M. S. Patterson and B. C. Wilson (2002) Direct near-infrared luminescence detection of singlet oxygen generated by photodynamic therapy in cells in vitro and tissues in vivo. *Photochem. Photobiol.* **75**, 382–391.
- Aveline, B. M., R. M. Sattler and R. W. Redmond (1998) Environmental effects on cellular photosensitization: correlation of phototoxicity mechanism with transient absorption spectroscopy measurements. *Photochem. Photobiol.* **68**, 51–62.
- Moan, J., S. Sandberg, T. Christensen and S. Elander (1983) Hematoporphyrin derivative: chemical composition, photochemical and photosensitizing properties. *Adv. Exp. Med. Biol.* **160**, 165–179.
- Pottier, R. and T. G. Truscott (1986) The photochemistry of haematoporphyrin and related systems. *Int. J. Radiat. Biol. Relat. Stud. Phys. Chem. Med.* **50**, 421–452.
- Kochevar, I. E. and R. W. Redmond (2000) Photosensitized production of singlet oxygen. *Methods Enzymol.* **319**, 20–28.
- Pogue, B. W., K. D. Paulsen, J. A. O'Hara, C. M. Wilmot and H. M. Swartz (2001) Estimation of oxygen distribution in RIF-1 tumors by diffusion model-based interpretation of pimonidazole hypoxia and eppendorf measurements. *Radiat. Res.* **155**, 15–25.
- Land, E. J., R. W. Redmond and T. G. Truscott (1986) On the nature of the active component of haematoporphyrin 'derivative'. *Cancer Lett.* **32**, 181–185.
- Ratcliffe, S. L. and E. K. Matthews (1995) Modification of the photodynamic action of delta-aminolaevulinic acid (ALA) on rat

- pancreatoma cells by mitochondrial benzodiazepine receptor ligands. *Br. J. Cancer* **71**, 300–305.
38. Verma, A., S. L. Facchina, D. J. Hirsch, S. Y. Song, L. F. Dillahey, J. R. Williams and S. H. Snyder (1998) Photodynamic tumor therapy: mitochondrial benzodiazepine receptors as a therapeutic target. *Mol. Med.* **4**, 40–45.
 39. Kessel, D. and Y. Luo (1999) Photodynamic therapy: a mitochondrial inducer of apoptosis. *Cell Death Differ.* **6**, 28–35.
 40. Mori, H. and A. K. Christensen (1980) Morphometric analysis of Leydig cells in the normal rat testis. *J. Cell Biol.* **84**, 340–354.
 41. Moan, J. and S. Sommer (1985) Oxygen dependence of the photosensitizing effect of hematoporphyrin derivative in NHIK 3025 cells. *Cancer Res.* **45**, 1608–1610.
 42. Mitchell, J. B., S. McPherson, W. DeGraff, J. Gamson, A. Zabell and A. Russo (1985) Oxygen dependence of hematoporphyrin derivative-induced photoinactivation of Chinese hamster cells. *Cancer Res.* **45**, 2008–2011.
 43. Huang, Z., Q. Chen, A. Shakil, H. Chen, J. Beckers, H. Shapiro and F. W. Hetzel (2003) Hyperoxygenation enhances the tumor cell killing of photofrin-mediated photodynamic therapy. *Photochem. Photobiol.* **78**, 496–502.
 44. Allison, R. R., C. Sibata, T. S. Mang, V. S. Bagnato, G. H. Downie, X. H. Hu and R. E. Cuenca (2004) Photodynamic therapy for chest wall recurrence from breast cancer. *Photodiagn. Photodyn. Ther.* **1**, 157–171.
 45. Schuh, M., U. O. Nseyo, W. R. Potter, T. L. Dao and T. J. Dougherty (1987) Photodynamic therapy for palliation of locally recurrent breast carcinoma. *J. Clin. Oncol.* **5**, 1766–1770.
 46. Khan, S. A., T. J. Dougherty and T. S. Mang (1993) An evaluation of photodynamic therapy in the management of cutaneous metastases of breast cancer. *Eur. J. Cancer* **29A**, 1686–1690.
 47. Li, K., J. Q. Lu, R. S. Brock, B. Yang and X. H. Hu (2005) Quantitative modeling of skin images using parallel Monte Carlo methods. *Proc. SPIE* **5693**, 82–87.
 48. Ding, H., J. Q. Lu, K. M. Jacobs and X. H. Hu (2005) Determination of refractive indices of porcine skin tissues and intralipid at 8 wavelengths between 325 and 1557 nm. *J. Opt. Soc. Am. A Opt. Image Sci. Vis.* **22**, 1151–1157.